

Ferroelectricity at ferroelectric domain walls

Jacek C. Wojdeł and Jorge Íñiguez

Institut de Ciència de Materials de Barcelona (ICMAB-CSIC), Campus UAB, 08193 Bellaterra, Spain

We present a first-principles study of model domain walls (DWs) in prototypic ferroelectric PbTiO_3 . At high temperature the DW structure is somewhat trivial, with atoms occupying high-symmetry positions. However, upon cooling the DW undergoes a symmetry-breaking transition characterized by a giant dielectric anomaly and the onset of a large and switchable polarization. Our results thus corroborate previous arguments for the occurrence of ferroic orders at structural DWs, providing a detailed atomistic picture of a temperature-driven DW-confined transformation. Beyond its relevance to the field of ferroelectrics, our results highlight the interest of these DWs in the broader areas of low-dimensional physics and phase transitions in strongly-fluctuating systems.

PACS numbers: 77.80.B-, 63.70.+h, 71.15.Mb

The structural domain walls (DWs) occurring in ferroelectric (FE) and ferroelastic (FS) materials have become a focus of attention. Recent studies show that the DWs can present a variety of properties, from conductive [1–4] and optical [5, 6] to magnetic [7–9], that differ from those of the neighboring domains, which suggests that they could be the active element in nano-technological applications [10, 11]. Elucidating the DW behavior poses major experimental challenges, and the origin of most of the newly discovered effects remains unclear. In fact, we still lack a detailed structural and dynamical picture of the DWs, and in many cases we can only speculate about the structure–property relationships at work within them. Hence, there is a pressing need for predictive theoretical studies tackling the DWs at an atomistic level and at the relevant conditions of temperature, etc.

The DW structure, and even the possible occurrence of DW-confined ferroic orders, have been discussed theoretically for decades, usually in the framework of continuum Ginzburg-Landau or phenomenological model theories [12–22]. Materials with competing structural instabilities have been a focus of attention, a good example being perovskite SrTiO_3 (STO). STO undergoes a FS transition driven by an anti-ferrodistortive (AFD) mode that involves concerted rotations of the O_6 octahedra in the perovskite structure. This mode competes with a FE instability that is suppressed by the onset of the AFD distortion [23]. Yet, there are both theoretical and experimental indications that a polar order occurs at low temperatures *within STO's FS DWs* [16, 24–26], i.e., in the region where the otherwise dominant AFD distortions vanish. In this context, it is worth noting recent first-principles studies predicting that PbTiO_3 (PTO) [27] and related compounds [28] present a FE-AFD competition that is even stronger than the one occurring in STO. These are the ideal conditions to obtain interesting effects at structural DWs, and motivated this work.

Low-temperature study.— We employed the tools of Ref. 27, which permit large-scale simulations with first-principles predictive power, to investigate an ideal version of the simplest DWs occurring in PTO, namely,

180° boundaries separating regions of opposed polarization and being perfectly planar. We used the model potential for PTO labeled “ L^I ” [27], which we briefly describe in [29]. As shown in Fig. 6(a), we set the polarization of the first domain \mathbf{P}^I parallel to the [100] direction of the perovskite lattice, and took $\mathbf{P}^{II} \parallel [\bar{1}00]$ for the second one; the DW in between was assumed to reside in a (001) plane. Our supercell, which contains $12 \times 12 \times 20$ perovskite units (14400 atoms), is periodically repeated and holds two DWs.

We investigated the ground state structure of this multi-domain configuration by means of Monte Carlo (MC) simulated annealings [29]. Figure 6(b) shows the x -component of the polarization (P_x) as we move along z . We observe two domains within which PTO adopts the structure of its homogeneous ground state, with an associated polarization of about 0.99 C/m^2 and a cell aspect ratio of about 1.07. The domains are separated by a DW centered at a PbO plane and presenting a thickness of about one unit cell.

Our DWs do not display any rotations of the O_6 octahedra. This result lends itself to a simple explanation: Because the DWs are ultra-thin, hypothetical DW-localized AFD modes would *overlap* with the neighboring FE distortions, and thus be penalized by the FE-AFD competition. As a result, the absence of localized AFD modes seems rather natural.

Nevertheless, the structure of the DWs is far from being trivial. As shown in Fig. 6(c), a non-zero P_y polarization appears at the DW plane and rapidly vanishes as we move into the domains. This DW polarization is switchable, as evidenced by the hysteresis loop in Fig. 2(a). Further calculations show that the polarizations of neighboring DWs couple, and tend to align in a parallel configuration when the walls are sufficiently close. However, the DW–DW interaction quickly decreases with the separation distance; for example, for our $12 \times 12 \times 20$ supercell, the energy split between the parallel and anti-parallel states is about 0.01 meV per DW cell, which is negligible. Hence, the anti-parallel configuration shown in Fig. 6 is a stable state (i.e., a local minimum of the

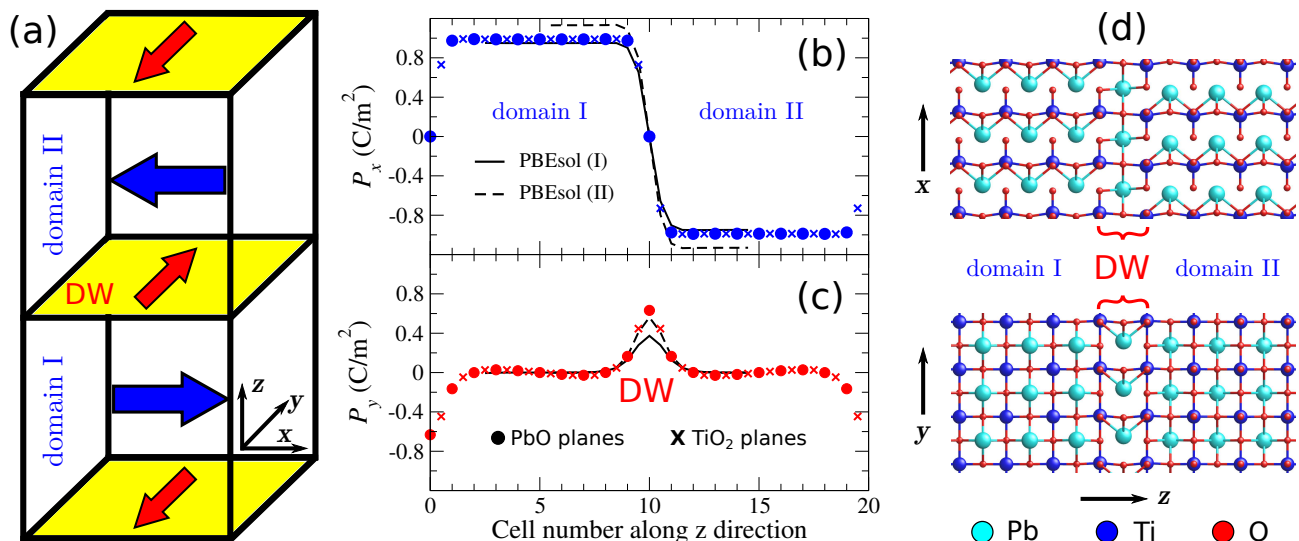


FIG. 1. Panel (a): Sketch of the supercell used in our simulations. The indicated Cartesian axes coincide with the principal directions of the perovskite lattice. Panels (b) and (c): Polarization profile corresponding to the stable structure of our multi-domain configuration. (Calculation of local polarizations described in Ref. [29].) The “PBEsol (I)” lines show the results of an unconstrained first-principles structural relaxation [29]; the agreement with the model predictions is essentially perfect for the P_x profile; for the DW polarization we obtain a slightly smaller value. The “PBEsol (II)” lines show the results of a first-principles relaxation in which the supercell lattice parameters were fixed to match those predicted by our model potential; the agreement for the P_y profile is essentially perfect; for the polarization within the domains we get slightly larger values. Panel (d): Views of the atomic structure of our multi-domain configuration.

energy), but not more significant than the also stable, quasi-degenerate parallel configuration.

Our results show how strain and the reduced dimensionality determine the energetics of the DW-confined FE distortion. The onset of the multi-domain structure for P_x implies a strong deformation of the perovskite lattice: it becomes tetragonal and acquires an aspect ratio of 1.07, the long lattice vector coinciding with the polar axis x . In the case of our simulated system, the xy plane is homogeneously strained throughout the supercell (stretched along x , shrunk along y). Hence, even if we have $P_x = 0$ at the DWs of Fig. 6, the strain disfavors the occurrence of a DW polarization along the y direction, which is subject to a compression. The ensuing effect can be appreciated in the potential wells of Fig. 2(b): Case I corresponds to the full development of the FE distortion of PTO, as it happens within the domains. Case II corresponds to the development of a three-dimensional y -polarized state when we constrain the cell to be strained as in the x -polarized FE state; the equilibrium polarization and associated energy gain get clearly reduced, and we obtain a value of P_y (about $0.75 C/m^2$) that is not far from our result at the DW center (about $0.65 C/m^2$). Additionally, Fig. 2(b) shows a case III corresponding to the condensation of P_y at our DWs; the energy well becomes shallower than in case II, indicating a further weakening of the polar instability caused by the spatial confinement (i.e., by the truncation of interactions favoring the three-dimensional homogeneous polar state) and the competi-

tion with the P_x distortion of the neighboring domains. Nevertheless, the obtained well depth (86 meV/cell) is sizable, which suggests that the predicted DW instability should occur at relatively high temperatures.

We checked the correctness of our model-potential predictions by running direct first-principles calculations of our multi-domain structure, using a $1 \times 1 \times 20$ cell. As shown in Figs. 6(b) and 6(c), the agreement between our model-potential and first-principles results is very good, and the FE character of PTO’s DWs is confirmed [30]. We should note that there are several first-principles studies of the 180° DWs of PTO in the literature [18, 31–33], and the consensus is that no DW-confined polarization occurs. We cannot be sure about the reasons why these previous works did not find polarized DWs; some possibilities are discussed in [29].

We checked whether this confined polarization occurs in other PTO DWs. We found that 180° DWs lying in other planes – e.g., a (011) boundary separating domains with $\mathbf{P}^I \parallel [100]$ and $\mathbf{P}^{II} \parallel [\bar{1}00]$ – present polar distortions analogous to the one just described. In contrast, we found that 90° DWs do not present any FE instability, a result probably related with the fact that these boundaries are considerably more distorted than their 180° counterparts, or to the elastic (epitaxial tensile) constraints we had to impose in order to stabilize them. PTO’s 90° DWs will be discussed elsewhere.

Finally, let us note that the low-temperature configuration of our PTO DWs can be described as being Bloch-

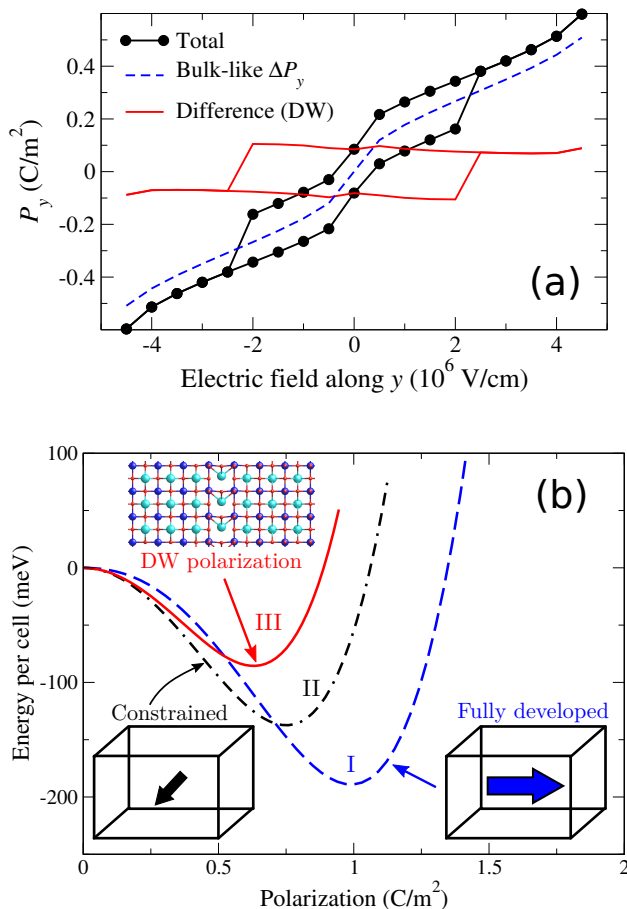


FIG. 2. Panel (a): Polarization loop computed for the x -polarized multi-domain state of Fig. 6 and for an electric field along the y direction. For these simulations we used a $1 \times 1 \times 20$ supercell, thus assuming an homogeneous switch, and performed the calculations in the limit of 0 K (details in [29]). The total response (black line and circles) is split in two parts: (1) The response of an x -polarized mono-domain state (dashed blue line); note that this response does not saturate, as the P_x polarization will eventually rotate to align with the field. (2) The difference between the total and the mono-domain results (solid red line), which captures the DW response. In order to observe the switch at the DWs, we imposed in the simulations the strain of the multi-domain ground state, and thus prevented the domain polarizations from fully aligning with the applied field for relatively small field values. Such a constraint is similar to the epitaxial one characteristic of thin films. Panel (b): Energy wells corresponding to FE instabilities in various situations described in the text. Note that the $P = 0$ state corresponds to a different atomistic configuration in each case. In the case of the DW polarization (red solid line) the energy is given *per cell* within the DW plane.

like. First-principles theory has predicted the occurrence of Bloch-like DW configurations in materials like LiNbO_3 [18] and BaTiO_3 in its rhombohedral phase [21].

Behavior with temperature.— We studied PTO DWs as a function of increasing temperature by running MC

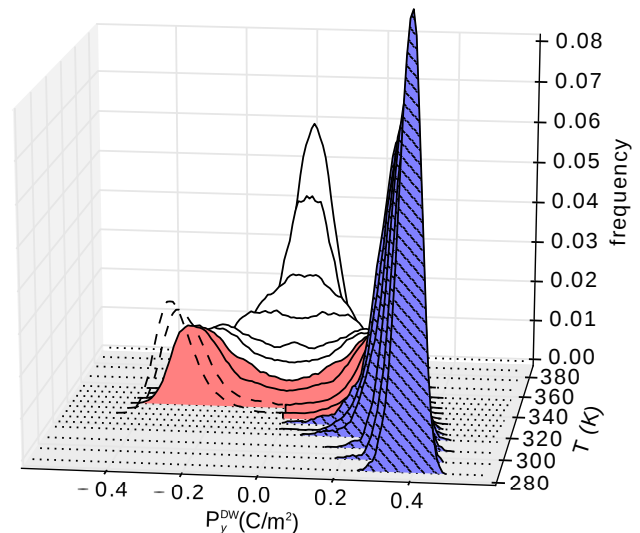


FIG. 3. Probability distribution $\rho(P_y^{\text{DW}})$ for the y -component of the polarization at the center of the DW and as a function of temperature. The three temperature regions mentioned in the text are marked with different colors: white for $T \geq 350$ K (where we clearly have $\langle P_y^{\text{DW}} \rangle = 0$), red for $320 \text{ K} < T < 350 \text{ K}$ (critical region), and blue with stripes for $T \leq 320$ K (where we clearly have $\langle P_y^{\text{DW}} \rangle \neq 0$). The left side of the histograms for $T = 330$ K and $T = 325$ K is drawn using dashed black lines; this is to emphasize that, at these temperatures, we attribute the P_y^{DW} fluctuations from positive to negative values to finite size effects (see [29]).

simulations as described in [29]. Figure 3 shows the obtained probability density, $\rho(P_y^{\text{DW}})$, for the y -component of the polarization at the DW plane. We observe three distinct regions: (1) For $T \leq 320$ K the DW presents a stable and large polarization, and the equilibrium state resembles the one discussed above. (2) For $T \geq 350$ K the DW gets disordered and we have a null thermal average $\langle P_y^{\text{DW}} \rangle = 0$. At those temperatures the system presents a mirror symmetry plane perpendicular to the y axis, and we could say that the DWs are in a *paraelectric* state [34]. (3) Finally, for $320 \text{ K} < T < 350 \text{ K}$ we have a narrow region in which, during the course of the MC simulation, P_y^{DW} occasionally switches between equivalent polar states. Clearly, the finite size of our simulation supercell is partly responsible for such fluctuations, which should be considered a spurious finite size effect below a certain transition temperature T_C^{DW} . At any rate, the presence of a phase transition is obvious from these results, and the analysis of the MC data suggests that we have $T_C^{\text{DW}} \approx 335$ K. (See [29] for details.)

The phase transitions in our simulated system are clearly appreciated in Fig. 4, which shows the evolution of the relevant order parameters and dielectric response. As the system cools down from high T , the diagonal components of the dielectric tensor increase sharply, revealing a FE transition at $T_C = 510$ K. [The quantitative disagreement between our computed T_C and the exper-

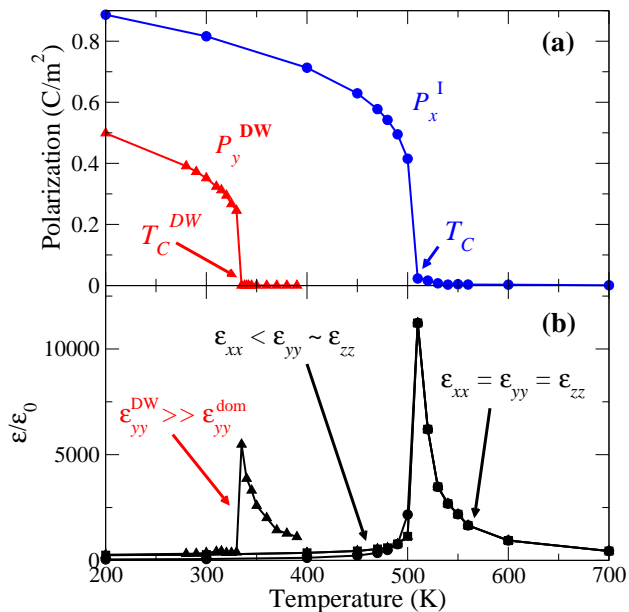


FIG. 4. Panel (a): Temperature dependent polarization at the center of the first domain (P_x^I , blue circles) and at the center of the DWs (P_y^{DW} , red triangles). Panel (b): Diagonal components of the dielectric permittivity tensor. The discontinuity for ϵ_{yy} (triangles) at $T = 390$ K is related with the finite-size effects described in [29].

imental result for PTO (760 K) is discussed in Ref. 27.] Note that for $T > 510$ K we have $\epsilon_{xx} = \epsilon_{yy} = \epsilon_{zz}$, reflecting the cubic symmetry of the paraelectric phase. Then, for $T \gtrsim T_C^{DW}$ the ϵ_{yy} component [triangles in Fig. 4(b)] behaves in an anomalous way. As regards the dielectric response along the y direction, our multi-domain configuration can be viewed as a set of parallel capacitors, so that the total dielectric constant can be split into domain and DW contributions, $\epsilon_{yy} = f^{dom}\epsilon_{yy}^{dom} + f^{DW}\epsilon_{yy}^{DW}$, where f^{dom} and f^{DW} are the respective volume fractions. Noting that $f^{dom} \approx 0.9$ and $f^{DW} \approx 0.1$ in our case, and that ϵ_{yy}^{dom} is featureless for $T < T_C$ (which we checked by running MC simulations of the mono-domain case), it is clear that the increase in ϵ_{yy} comes from a very large DW response ϵ_{yy}^{DW} . Hence, the DW-confined transition is driven by a FE soft mode and characterized by very strong fluctuations of the order parameter, as consistent with the reduced dimensionality.

Final remarks.— As mentioned, the possibility of having polar orders and dielectric anomalies associated with DWs has been discussed in the theoretical literature, typically employing phenomenological continuum models [16, 22]. Our first-principles work corroborates that such effects can indeed occur, providing for the first time a realistic atomistic picture of a T -driven DW-confined ferroic transformation.

One might describe the found transition as a change in the DW character, from Bloch to Ising, upon heating;

in fact, some authors have discussed similar effects in these terms [20, 22]. However, we think that our result is better described as a proper FE phase transition confined to the DW, to emphasize that it results in a switchable DW polarization. For the same reasons, we would rather denote the low-temperature state as a ferroelectric DW, and not simply as a DW with Bloch-like character. Note that, as in the case of LiNbO₃ [18], Bloch-like DWs may not display a net polarization.

The present results are the first step in the investigation of such an interesting phenomenon. Aspects for future work include: the possible critical behavior of the transition, the pre-translational dynamics, the internal structure of the DWs (can we have multi-domain states within them?), and the role of DW–DW interactions (can it affect the dimensionality and features of the transition?). We thus believe our findings will open exciting research avenues in the fields of phase transitions and low-dimensional physics.

It may seem surprising that the predicted effect has not been reported experimentally. However, note that observing such a FE order may require some uncommon measurements. Ideally, one would like to work with samples presenting a pattern of highly-ordered stripe domains separated by 180° DWs, as displayed by suitably grown PTO films [35] and PTO/STO superlattices [36, 37]. High-resolution X-ray measurements at low temperatures may reveal the DW order. Additionally, by measuring the dielectric response along the in-plane direction of the DWs, one should be able to observe a clear feature around T_C^{DW} . We hope our results will motivate further experimental work to characterize FE DWs and the transitions that may occur within them.

Work supported by MINECO-Spain (Grants No. MAT2010-18113 and No. CSD2007-00041) and CSIC [JAE-doc program (JCW)]. Some figures were prepared using VESTA [38]. We thank Ekhard Salje, David Vanderbilt, and Pavlo Zubko for their useful comments.

SUPPLEMENTAL INFORMATION FOR “FERROELECTRIC TRANSITIONS AT FERROELECTRIC DOMAIN WALLS”

In the following we describe the simulation methods employed as well as various technicalities pertaining to the calculation of some quantities. We also comment on the determination and quantitative accuracy of the temperature at which the domain wall-confined ferroelectric transition takes place, and on previous first-principles literature on the DWs in PbTiO₃.

METHODS

For most simulations we used the first-principles model for PTO described in Ref. 27, where it is labeled “ L^I ”. This model can be viewed as a Taylor series of the energy, around the ideal cubic perovskite structure, as a function of all possible atomic distortions and strains. The series was truncated at 4th order and only pairwise interaction terms were included. The potential parameters were computed by using the local density approximation (LDA) to density functional theory (DFT). To compensate for LDA’s well-known overbinding problem, we simulate the model under the action of a tensile hydrostatic pressure of 14.9 GPa.

We ran some direct first-principles simulations to verify the model predictions at low temperatures. For that task, we used the PBEsol[39] approach to DFT as implemented in the VASP package.[40] Note that the PBEsol functional has been shown to render accurate results for the equilibrium structures of several FE perovskite oxides[41] including PTO (which we checked ourselves). We used the projector augmented wave method to represent the ionic cores,[42, 43] solving for the following electrons: Ti’s $3p$, $3d$, and $4s$; Pb’s $5d$, $6s$, and $6p$; and O’s $2s$ and $2p$. Wave functions were represented in a plane-wave basis truncated at 500 eV, and a $6 \times 6 \times 1$ k -point grid was used for integrations within the Brillouin zone corresponding to a $1 \times 1 \times 20$ supercell. To better compare our model-potential and first-principles results, we conducted PBEsol structural relaxations in both an unconstrained way [“PBEsol (I)” results in Fig. 1 of our manuscript] and by imposing lattice vectors obtained from model-potential calculations [“PBEsol (II)”].

For the sake of comparison, we also ran some simulations at the LDA level, all other technicalities being identical to those of our PBEsol calculations.

We computed the electric dipoles caused by the displacement of individual atoms within a linear approximation, using the corresponding dynamical charge tensors as computed for the cubic phase. To compute Ti-centered local polarizations associated to specific cells, as those shown in Fig. 1, we proceeded in the following way: We summed up the dipoles associated to the central titanium and to its nearest-neighboring atoms (i.e., 6 oxygens and 8 leads), weighting the contribution of the neighbors appropriately (e.g., since an oxygen atom is shared by two Ti atoms, it contributes one half of its associated dipole to the polarization centered at each of its two neighboring titaniums). We proceeded analogously to compute Pb-centered polarizations. This is a rather standard scheme[32] related with the local-mode construction in classic first-principles models of ferroelectrics.[44]

Finally, we used a standard Monte Carlo (MC) scheme to account for the effect of temperature in our system, working with a periodically repeated box of $12 \times 12 \times 20$

PTO unit cells. At all temperatures we initialized our MC simulations from the multi-domain ground state configuration described in Fig. 1. We typically ran 25,000 MC sweeps for thermalization, followed by at least 25,000 additional sweeps for computing thermal averages. In the region of the DW-confined phase transition, marked in red in Fig. 3 of our manuscript, we did production runs of up to 150,000 MC sweeps, as needed to obtain acceptable statistics for $\rho(P_y^{\text{DW}})$. Note that, because of the quasi-two-dimensional and strongly-fluctuating nature of the polar order at the walls, this was an especially challenging task; in particular, as discussed below, our ability to get quantitatively accurate results in the critical region is limited by the size of the considered supercell, which is the largest we can afford with our current simulation tools. We also ran a simulation of the FE phase transition of PTO, always in a mono-domain configuration, using a $12 \times 12 \times 12$ simulation box periodically repeated. In this case, we always started the simulations from a perfectly cubic structure; then we ran 10,000 MC sweeps for thermalization, followed by 50,000 sweeps for computing averages, which was enough to obtain well converged results at all temperatures. We checked that the temperature dependent mono-domain polarization thus computed is essentially identical to the local polarization obtained at the middle of the domains in our multi-domain simulations.

Whenever we needed to run a structural relaxation with our model potential, we performed MC simulated annealings in which we reduced the temperature down to essentially 0 K, allowing the simulation to evolve until the system would get *frozen* at an energy minimum. In some cases we started the annealings at very low temperatures, which allowed us to investigate local (meta-stable) minima of the energy, as the lack of thermal activation prevents the simulated system from evolving to its most stable configuration. This was important, for example, to compute the hysteresis loops of Fig. 2(a) of our manuscript, as we needed to follow the evolution of the polar states, as a function of the magnitude of an opposing electric field, up to their meta-stability limit. Beyond that limit, the local energy minimum is lost and the relaxation (i.e., the simulated annealing) naturally evolves towards the polar state favored by the applied field. Using the same strategy, we were also able to quantify the energy gap between the states with parallel and anti-parallel DW polarizations, and thus determine that the DW–DW interaction is negligible for the separating distance (i.e., 9 unit cells or about 35 Å) corresponding to our simulation box.

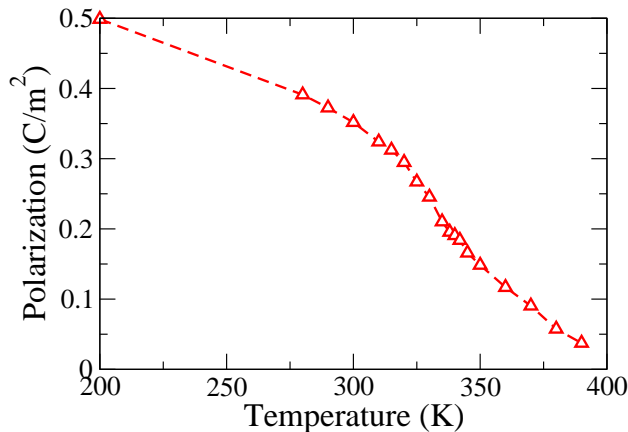


FIG. 5. Computed temperature dependence of $\langle |P_y^{\text{DW}}| \rangle$, the absolute value of the y component of the DW polarization. From the inflection point of this curve, obtained numerically, we can estimate $T_C^{\text{DW}} \approx 332$ K.

FINITE SIZE EFFECTS IN THE MONTE CARLO SIMULATIONS

As already mentioned in the manuscript, at temperatures around the DW-confined transition our MC results are affected by the fact that our simulation supercell is finite in size. More specifically, we simulate DWs that are composed of 12×12 cells periodically repeated in the DW plane. While we have checked that a lateral size of 12 cells is sufficient to describe the bulk FE transition of PTO with good accuracy, our results suggest that we may not be converged size-wise as regards the DW-confined transformation (see Fig. 3 of our manuscript). Whenever one deals with low-dimensional orders, large amplitude fluctuations are more likely to occur, which complicates convergence with size. Unfortunately, at present our software does not allow us to further increase the size of the simulation box, as the calculations become too heavy computationally. Nevertheless, an analysis of the results obtained for 12×12 DWs allows us to bracket T_C^{DW} quite precisely.

First of all, let us stress that the uncertainty caused by these size effects is of little practical importance. The affected temperature range is relatively small, approximately from 320 K to 350 K. Hence, from the point of view of comparing our value of T_C^{DW} with an eventual experimental determination, the error coming from size effects can be considered negligible.

There are simple and usually effective strategies to estimate the temperature dependence of the order parameter, from our MC data, in ways that are robust against size effects. Thus, for example, if we are interested in the thermal average of the DW polarization $\langle P_y^{\text{DW}} \rangle$, it is a good idea to compute the average of its absolute value, $\langle |P_y^{\text{DW}}| \rangle$, instead. In this way, spurious fluctuations (i.e., *jumps* between equivalent energy wells) of the DW po-

larization, permitted by the finite size of the simulation box, will not result in a vanishing order parameter. An obvious drawback of this approach is that $\langle |P_y^{\text{DW}}| \rangle$ will be different from zero even in the disordered phase, which is not correct. Yet, monitoring the temperature dependence of this quantity is usually enough to locate a phase transition, and even permits a quantitative estimation of the transition temperature.

Figure S1 shows the results for $\langle |P_y^{\text{DW}}| \rangle$ from our MC simulations. As expected, we obtain a smooth temperature dependence that clearly points at a transition occurring in the range between 320 K and 350 K. Further, we can estimate the transition temperature by numerically calculating the inflection point of this curve, which happens at about 332 K.

We were not fully satisfied by this simple estimate, and tried to analyze our MC data in more detail, proceeding as follows. Figure S2(a) shows the computed $\rho(P_y^{\text{DW}})$ evaluated at $P_y^{\text{DW}} = 0$ and as a function of temperature. There we can appreciate that at $T \leq 320$ K the DWs do not visit the $P_y^{\text{DW}} = 0$ state, as we have $\rho(0) \approx 0$. Hence, it is clear that our simulations predict $T_C^{\text{DW}} > 320$ K. Above that temperature, there is a range in which we get very small but non-zero values of $\rho(0)$, as well as a bimodal shape for $\rho(P_y^{\text{DW}})$. Do we really have disordered DWs at these temperatures?

To gain insight into the behavior of the system in this temperature range, we considered several ways to compute the dielectric constant ϵ_{yy} . Let us recall that $\epsilon_{yy} = \epsilon_0(\chi_{yy} + 1)$, and that we have

$$\epsilon_0 \chi_{yy} = \frac{\partial P_y}{\partial E_y} = \frac{\beta}{V} (\langle P_y^2 \rangle - \langle P_y \rangle^2), \quad (1)$$

where E_y is the applied electric field, V is the supercell volume, $\beta = 1/k_B T$, k_B is the Boltzmann constant, and $\langle \dots \rangle$ denotes a thermal average as computed from our MC simulations. Now, instead of using all the sweeps of our production MC runs to compute χ_{yy} , it was instructive to consider smaller sets of data that we label by i , compute the corresponding $\chi_{yy}^{(i)}$ for each set, and perform a statistical analysis of the results. Figure S2(b) summarizes the outcome of such an exercise. We show the results obtained by considering sets of data composed of 16,000 MC sweeps each. (We checked that 16,000 sweeps are typically sufficient to get well-converged thermal averages of our quantities of interests.) If we approximate χ_{yy} by

$$\bar{\chi}_{yy} = \frac{1}{M} \sum_{i=1}^M \chi_{yy}^{(i)}, \quad (2)$$

where M is the number of 16,000-sweep sets that we have, we obtain the results shown by a solid black line and triangles in Fig. S2(b). Interestingly, $\bar{\chi}_{yy}$ presents two

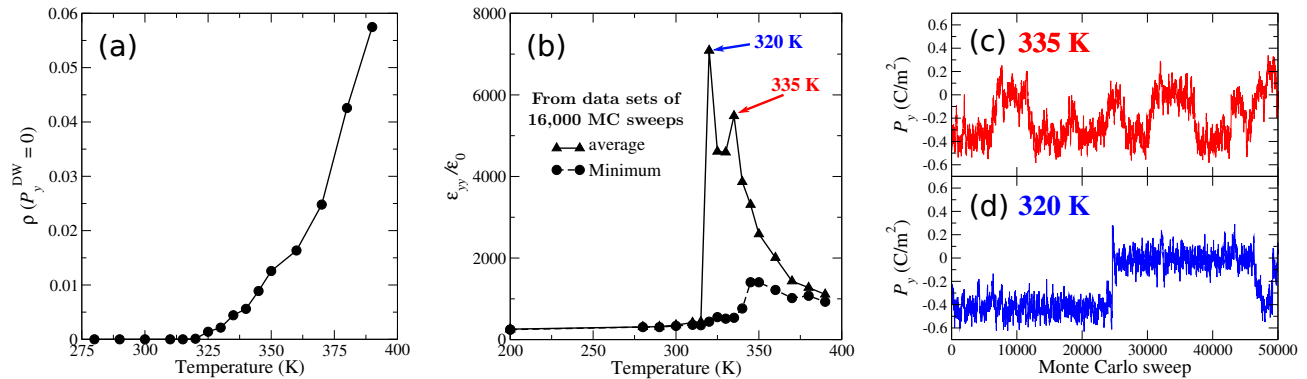


FIG. 6. Panel (a): Probability $\rho(0)$ of having $P_y^{\text{DW}} = 0$ as a function of temperature. Panel (b): ϵ_{yy} component of the dielectric permittivity tensor, as a function of temperature, and estimated in the two different ways described in the text. Panels (c) and (d): Evolution of P_y during 50,000 sweeps of the MC runs at 335 K and 320 K, respectively. The shown data is representative of the behavior of our simulated system during the longer runs.

peaks located at 320 K and 335 K, respectively. If, alternatively, we approximate χ_{yy} by

$$\chi_{yy}^{\min} = \min_i \chi_{yy}^{(i)}, \quad (3)$$

we get the results shown by a dashed black line and circles in Fig. S2(b). In this case, we get a single broad peak with a maximum at $T \approx 340$ K.

To understand the origin of these results, it is useful to look at the evolution of P_y during the MC runs, as shown in Figs. S2(c) and S2(d) for 335 K and 320 K, respectively. At 335 K we observe frequent fluctuations in the value of P_y , suggesting that the DWs are not ordered. (Note that we have two DWs in the simulation cell; at 335 K we get $|P_y| \approx 0.4$ C/m² when the two DW polarizations are parallel, and $|P_y| \approx 0$ when they are anti-parallel.) The fluctuations are large, which leads to a large response according to Eq. (1) and explains the peak that $\bar{\chi}_{yy}$ presents at that temperature. At the same time, it is possible to find relatively long segments of the MC run in which P_y fluctuates around a constant value. Hence, the computed χ_{yy}^{\min} is much smaller than $\bar{\chi}_{yy}$.

Figure S2(d) shows that the situation at 320 K is very different. In this case, our DWs clearly present a stable polarization. Nevertheless, from time to time we do observe a jump in P_y , indicating a switch in the polarization of one of the DWs. These infrequent jumps lead to a very large value of $\bar{\chi}_{yy}$, which peaks at that temperature. In contrast, we find that χ_{yy}^{\min} , which is obviously determined by a segment of the MC trajectory that is free of jumps in P_y , takes a relatively small value. From this analysis, we can conclude that the peak observed at 320 K in $\bar{\chi}_{yy}$ is an artifact associated to the finite size of our simulation supercell, and that our results suggest that T_C^{DW} is about 335 K or 340 K. To generate the figures in our manuscript, we assumed $T_C^{\text{DW}} = 335$ K and processed our MC data accordingly.

Finally, let us note another feature of our results that

is related with the finite size of our simulation box. In Fig. 4(b) of our manuscript, the results for ϵ_{yy} with a clear DW contribution extend only up to $T \approx 390$ K, where a discontinuity can be appreciated. The reason is that above that temperature, because of the finite size our supercell, the initial multi-domain configuration evolves during the MC run into a mono-domain state, which is more stable for the elastic (unconstrained) and electrical (short-circuit) boundary conditions considered in our simulations. Nevertheless, we do not observe any sort of structural order at the DWs for $T \gtrsim T_C^{\text{DW}}$, and have no reason to expect a different behavior at higher temperatures. Hence, our current inability to investigate the DWs up to T_C is not troublesome.

FIRST-PRINCIPLES AND MODEL-POTENTIAL ACCURACY

The largest quantitative uncertainty affecting our value for T_C^{DW} is surely related with the inaccuracies inherent to our first-principles model potentials. As shown in Ref. 27, our potential for PTO reproduces the energetics of the FE instabilities with very good accuracy, and it also accounts well for the lowest-energy perturbations of the relevant stable structures. Hence, as far as the homogeneous FE phases of the material are concerned, our potential can be considered an accurate approximation to density functional theory (DFT) results obtained using the local density approximation (LDA). However, the computed $T_C = 510$ K turns out to be significantly smaller than the experimental value of 760 K, which suggests there is a problem with the accuracy of the LDA and employed first-principles methods. As discussed in Ref. 27, tracking down the origin of this error is not trivial; the LDA could be giving us (1) FE instabilities that are too weak, (2) AFD instabilities that are too strong, (3) a FE-AFD competition that is too strong, or (4) a

combination of all these problems. All such errors will affect our calculation of T_C^{DW} in essentially the same way as they affect the calculation of T_C . Hence, we have reasons to believe that our model may underestimate significantly the temperature of the DW-confined transition.

Additionally, one may wonder whether our model reproduces the DFT energetics associated with the DWs as well as it captures those related with the bulk FE state. Our model renders a DW energy $E^{\text{DW}} = 107 \text{ mJ/m}^2$ when we allow for a full structural relaxation of the DW, and $E^{\text{DW}} = 190 \text{ mJ/m}^2$ when we constrain the DW to remain in the unpolarized high-symmetry state. Using the PBEsol approach to DFT [which we denote “PBEsol (I)” in our manuscript; see Methods section], we get 149 mJ/m^2 and 152 mJ/m^2 , respectively, for these two quantities. When we run the PBEsol relaxation imposing the cell strain obtained from our model calculations [“PBEsol (II)”], we get 225 mJ/m^2 and 250 mJ/m^2 , respectively. Note that Meyer and Vanderbilt reported a value of 132 mJ/m^2 for this quantity,[32] which they computed at the LDA level and considering an unpolarized DW. Thus, we can conclude that our model gives acceptable results for the DW energy, even though this piece of information was not used when calculating the potential parameters. (For reference, we ran LDA calculations considering an unpolarized DW, as done in Ref. 32, and got a DW energy of 97 mJ/m^2 .)

For us it is more relevant to consider the energy difference between the paraelectric and ferroelectric states of the DW, i.e., the depth of the energy well corresponding to case III in Fig. 2(b) of our manuscript. For this quantity we get 86 meV/cell with our model, 4 meV/cell at the “PBEsol (I)” level, and 26 meV/cell at the “PBEsol (II)” level. It is interesting to note that, despite the good agreement for the DW polarization and structure between our model and the PBEsol calculations [see Fig. 1(c)], the differences in energy are large. This comparison suggests that, with respect to the result one would obtain from a PBEsol simulation, our model may overestimate significantly the value of T_C^{DW} . [For reference, we also computed the depth of the energy well corresponding to the DW-confined FE instability at the LDA level, and obtained 6 meV/cell when a full structural relaxation is allowed, and 45 meV/cell when the cell obtained from our model-potential simulations is imposed. Hence, LDA renders slightly stronger DW-confined instabilities than PBEsol.]

How worrisome are the differences between our model and PBEsol energetics as regards the DW order? How well would a PBEsol simulation reproduce the T_C of the FE transition occurring in the bulk of PTO? Is PBEsol the best DFT flavor available for this task? It is not possible to answer those questions at present. As an indication, let us mention that our PBEsol calculations render a value of 67 meV/cell for the energy difference between the bulk-paraelectric and bulk-ferroelectric phases of PTO.

This value corresponds to the depth of the energy well of case I in Fig. 2(b), for which we get 189 meV/cell using our model. Hence, since our model underestimates PTO’s experimental T_C quite significantly, we can tentatively conclude that a PBEsol simulation would lead to very small Curie temperature for this material. Hence, despite its accuracy at predicting equilibrium structures, it is not clear at all whether PBEsol should be our DFT method of choice for calculating the energetics of PTO’s FE instabilities.

We hope this discussion illustrates the difficulties involved in assessing the accuracy of DFT, and DFT-based methods, as regards the calculation of transition temperatures in materials with non-trivial structural and lattice-dynamical effects like PTO. As mentioned, we have reasons to think that our result for T_C^{DW} might be smaller than the experimental value, and we also have reasons to think it might be larger. At any rate, the existence of a DW-confined polar order and temperature-driven transition remains a solid prediction.

RELATION TO PREVIOUS LITERATURE

As mentioned in our paper, there are several first-principles studies of the 180° DWs of PTO available in the literature [18, 31–33]. Interestingly, except for the earliest one,[31] all of them suggest that no polar order occurs within the DW plane. We cannot be sure about the reasons why these previous works did not find polarized DWs, but some possibilities are worth mentioning. First, it is usual in studies of this sort to assume a simplification of the DW structure, typically imposing that the symmetry operations that are common to the two neighboring domains be preserved in the structural relaxations. Such an approximation, which is adopted to alleviate the computational cost of the simulations, may well render a null DW polarization. Second, we obtained our polar DW configurations from MC annealings based on our PTO potential, which allowed us to explore the configuration space very efficiently, and used such structures as the starting point of the first-principles relaxations. In our experience, one is not guaranteed to reach such a distorted structure in a typical first-principles optimization, which would start from the non-polar DW state, even if all symmetries are broken. (Note that the information on the energetics of the DW instability, given in Section III above, may be relevant to this issue.)

Let us also note that, recently, Wei *et al.* [45] have found polar distortions at the structural (antiphase) DWs of non-polar compound PbZrO_3 . Wei *et al.* present first-principles results showing the bi-stability of the polar DW configuration, and thus argue that such a polarization is switchable. However, the supplemental material of Ref. 45 suggests that the switch of the DW polarization also involves the reversal of structural distortions

inside the domains. This is reminiscent of the so-called *hybrid improper ferroelectrics* – where the polarization switch must be accompanied by the reversal of one additional order parameter [46–49] – and of the polar order predicted at the FS walls of CaTiO_3 [17]. In contrast, the polarization of our PTO DWs can switch without affecting the surrounding domains.

-
- [1] J. Seidel, L. W. Martin, Q. He, Q. Zhan, Y. H. Chu, A. Rother, M. E. Hawkrige, P. Maksymovych, P. Yu, M. Gajek, N. Balke, S. V. Kalinin, S. Gemming, F. Wang, G. Catalan, J. F. Scott, N. A. Spaldin, J. Orenstein, and R. Ramesh, *Nature Materials* **8**, 229 (2009).
- [2] J. Guyonnet, I. Gaponenko, S. Gariglio, and P. Paruch, *Advanced Materials* **23**, 5377 (2011).
- [3] S. Farokhipoor and B. Noheda, *Physical Review Letters* **107**, 127601 (2011).
- [4] A. Aird and E. K. H. Salje, *Journal of Physics: Condensed Matter* **10**, L377 (1998).
- [5] S. Y. Yang, J. Seidel, S. J. Byrnes, P. Shafer, C. H. Yang, M. D. Rossell, P. Yu, Y. H. Chu, J. F. Scott, J. W. Ager, L. W. Martin, and R. Ramesh, *Nature Nanotechnology* **5**, 143 (2010).
- [6] M. Alexe and D. Hesse, *Nature Communications* **2** (2011), 10.1038/ncomms1261.
- [7] Q. He, C. H. Yeh, J. C. Yang, G. Singh-Bhalla, C. W. Liang, P. W. Chiu, G. Catalan, L. W. Martin, Y. H. Chu, J. F. Scott, and R. Ramesh, *Physical Review Letters* **108**, 067203 (2012).
- [8] M. Daraktchiev, G. Catalan, and J. F. Scott, *Physical Review B* **81**, 224118 (2010).
- [9] Z. V. Gareeva and A. K. Zvezdin, *Physics of the Solid State* **52**, 1714 (2010).
- [10] E. K. Salje, *ChemPhysChem* **11**, 940 (2010).
- [11] G. Catalan, J. Seidel, R. Ramesh, and J. F. Scott, *Reviews of Modern Physics* **84**, 119 (2012).
- [12] B. Strukov and A. Levanyuk, *Ferroelectric Phenomena in Crystals: Physical Foundations* (Springer, 1998).
- [13] A. Tagantsev, L. E. Cross, and J. Fousek, *Domains in Ferroic Crystals and Thin Films* (Springer, 2010).
- [14] J. J. Lajzerowicz and J. J. Niez, *Journal de Physique Letters* **40**, L165 (1979).
- [15] B. Houchmandzadeh, J. Lajzerowicz, and E. Salje, *Journal of Physics: Condensed Matter* **3**, 5163 (1991).
- [16] A. K. Tagantsev, E. Courtens, and L. Arzel, *Physical Review B* **64**, 224107 (2001).
- [17] L. Goncalves-Ferreira, S. A. T. Redfern, E. Artacho, and E. K. H. Salje, *Physical Review Letters* **101**, 097602 (2008).
- [18] D. Lee, R. K. Behera, P. Wu, H. Xu, Y. L. Li, S. B. Sinnott, S. R. Phillpot, L. Q. Chen, and V. Gopalan, *Phys. Rev. B* **80**, 060102 (2009).
- [19] S. Conti, S. Müller, A. Poliakovsky, and E. K. H. Salje, *Journal of Physics: Condensed Matter* **23**, 142203 (2011).
- [20] V. Stepkova, P. Marton, and J. Hlinka, *Journal of Physics: Condensed Matter* **24**, 212201 (2012).
- [21] M. Taherinejad, D. Vanderbilt, P. Marton, V. Stepkova, and J. Hlinka, *Physical Review B* **86**, 155138 (2012).
- [22] P. Marton, V. Stepkova, and J. Hlinka, *Phase Transitions* **86**, 103 (2013).
- [23] W. Zhong and D. Vanderbilt, *Physical Review Letters* **74**, 2587 (1995).
- [24] J. F. Scott, E. K. H. Salje, and M. A. Carpenter, *Physical Review Letters* **109**, 187601 (2012).
- [25] E. A. Eliseev, A. N. Morozovska, Y. Gu, A. Y. Borisevich, L.-Q. Chen, V. Gopalan, and S. V. Kalinin, *Physical Review B* **86**, 085416 (2012).
- [26] E. K. H. Salje, O. Aktas, M. A. Carpenter, V. V. Laguta, and J. F. Scott, *Physical Review Letters* **111**, 247603 (2013).
- [27] J. C. Wojdel, P. Hermet, M. P. Ljungberg, P. Ghosez, and J. Íñiguez, *Journal of Physics: Condensed Matter* **25**, 305401 (2013).
- [28] I. A. Kornev, L. Bellaiche, P.-E. Janolin, B. Dkhil, and E. Suard, *Physical Review Letters* **97**, 157601 (2006).
- [29] Please see the online Supplemental Materials for a brief description of various technicalities of our calculations and some complementary results and analysis.
- [30] For the FE phase of PTO, our model potential predicts long and short lattice constants of 4.21 Å and 3.94 Å, respectively. In contrast, our PBEsol calculations render 4.03 Å and 3.87 Å for these quantities. These results are consistent with those in Figs. 6(b) and 6(c), as the smaller lattice parameters lead to relatively small polar distortions, both in the domains and within the DWs, in the PBEsol (I) case.
- [31] S. Pöykkö and D. J. Chadi, *Applied Physics Letters* **75**, 2830 (1999).
- [32] B. Meyer and D. Vanderbilt, *Physical Review B* **65**, 104111 (2002).
- [33] L. He and D. Vanderbilt, *Physical Review B* **68**, 134103 (2003).
- [34] In this high- T regime, the DW presents all the symmetries that are common to its neighboring domains.
- [35] S. K. Streiffer, J. A. Eastman, D. D. Fong, C. Thompson, A. Munkholm, M. V. Ramana Murty, O. Auciello, G. R. Bai, and G. B. Stephenson, *Physical Review Letters* **89**, 067601 (2002).
- [36] P. Zubko, N. Stucki, C. Lichtensteiger, and J. M. Triscone, *Physical Review Letters* **104**, 187601 (2010).
- [37] P. Zubko, N. Jecklin, A. Torres-Pardo, P. Aguado-Puente, A. Gloter, C. Lichtensteiger, J. Junquera, O. Stéphan, and J. M. Triscone, *Nano Letters* **12**, 2846 (2012).
- [38] K. Momma and F. Izumi, *Journal of Applied Crystallography* **41**, 653 (2008).
- [39] J. Perdew, A. Ruzsinszky, G. Csonka, O. Vydrov, G. Scuseria, L. Constantin, X. Zhou, and K. Burke, *Physical Review Letters* **100**, 136406 (2008).
- [40] G. Kresse and J. Furthmüller, *Physical Review B* **54**, 11169 (1996).
- [41] R. Wahl, D. Vogtenhuber, and G. Kresse, *Physical Review B* **78**, 104116 (2008).
- [42] P. E. Blöchl, *Physical Review B* **50**, 17953 (1994).
- [43] G. Kresse and D. Joubert, *Physical Review B* **59**, 1758 (1999).
- [44] W. Zhong, D. Vanderbilt, and K. M. Rabe, *Physical Review B* **52**, 6301 (1995).
- [45] X.-K. Wei, A. K. Tagantsev, A. Kvasov, K. Roleder, C.-L. Jia, and N. Setter, *Nature Communications* **5** (2014), 10.1038/ncomms4031.
- [46] E. Bousquet, M. Dawber, N. Stucki, C. Lichtensteiger,

- P. Hermet, S. Gariglio, J.-M. Triscone, and P. Ghosez, *Nature* **452**, 732 (2008).
- [47] N. A. Benedek and C. J. Fennie, *Physical Review Letters* **106**, 107204 (2011).
- [48] Z. Zanolli, J. C. Wojdeł, J. Íñiguez, and P. Ghosez, *Physical Review B* **88**, 060102 (2013).
- [49] Y. Yang, J. Íñiguez, A.-J. Mao, and L. Bellaiche, *Physical Review Letters* **112**, 057202 (2014).